Supporting Information

Ag Nanoparticle-Decorated $Co(OH)_2$ Nanowires for Efficient Electrocatalytic Nitrate Reduction to Ammonia

Lili Zhang [1], Yifan Li [1], Qian Bai [2], Runmin Li [1,2] and Huishan Shang [1,*]

[1] School of Chemical Engineering, Zhengzhou University, Zhengzhou 450001, China
[2] Energy & Catalysis Center, School of Materials Science and Engineering, Beijing Institute of Technology, Beijing 100081, China
* Correspondence: shanghs@zzu.edu.cn

1. Characterization

X-ray diffraction (XRD, Bruker D8 Advance, scan range of 10-80°) analyses were performed to determine the crystallinity and phase of samples. X-ray photoelectron spectroscopy (XPS) was carried out on the Escalab 250Xi electron spectrometer using Mg Kα radiation. Scanning electron microscopy (SEM) images were obtained from Ultra 55Zeiss field emission scanning electron microscope. Transmission electron microscopy (TEM), high-angle annular dark-field scanning TEM (HAADF-STEM), and energy dispersive spectroscopy (EDS) results were performed by using an FEI Talos F200S with an acceleration voltage of 200 kV. The nitrogen adsorption-desorption isotherms were collected on the Quantachrone Autosorb iQ-MP-C. Specific surface areas and pore-size distributions were calculated based on Brunauer-Emmett-Teller (BET) and Barrett-Joyner-Halenda (BJH) analyses, respectively.

2. Electrochemical measurements

All potentials were calibrated to the RHE by the following equation:

$$E_{RHE}=E_{Hg/HgO}+0.0591\times pH+\varphi_{\text{referene}}$$

The NH_3 Faradaic efficiency was calculated according to

$$FE_{NH3}=\frac{Q_{NH3}}{Q}=\frac{n_{NH3}Vc_{NH3}F}{Q}$$

where Q represents the applied overall coulomb quantity (C), Q_{NH3} is the coulomb required to produce NH_3, n is the electron-transfer number (for 1 mol NH_3, it is 8), V is the volume of the catholyte of the cathode chamber (45 mL), cNH_3 is the concentration of NH_3 produced, and F is the Faraday constant (96485 C mol^{-1}).

The pseudo-first-order rate constants for the two consecutive steps of nitrate reduction:

$$NO_3^- \rightarrow NO_2^-(k_1)$$

$$NO_2^- \rightarrow NH_3^-(k_1)$$

Assuming excess proton/electron supply under constant potential, both steps follow pseudo-first-order kinetics.

For NO_3^- reduction (k_1):

$$\frac{d[NO_3^-]}{dt} = -k_1[NO_3^-] \Rightarrow \ln[NO_3^-] = \ln[NO_3^-]_0 - k_1 t$$

Thus, k_1 is obtained from the slope of the linear fit of ln[NO3-] versus time.

For NO_2^- reduction (k_2):

$$\frac{d[NO_2^-]}{dt} = -k_2[NO_2^-] \Rightarrow \ln[NO_2^-] = \ln[NO_2^-]_0 - k_2 t$$

Similarly, k_2 is extracted from the slope of ln[NO_2^-] versus time when NO_2^- is used as the sole reactant.

Determination of ammonia (NH_4^+)

UV-vis spectrophotometer was used to detect the ion concentration of pre- and post-test electrolytes after diluting to the appropriate concentration to match the range of calibration curves. The standard curve can be generated by examining the UV-Vis spectra of solutions with varying concentrations of NH4+. Typically, an appropriate amount of electrolyte was taken out from the cathode chamber and diluted into appropriate concentration. 2 mL of salicylic acid solution (5 wt% salicylic acid and 5 wt % sodium citrate was dissolved in 1 M sodium hydroxide solution), 1 mL of 0.05 M sodium hypochlorite solution and 0.2 mL of 1 wt % sodium nitrite ferricyanide solution were added to the above diluted electrolyte. After the mixed electrolyte solution was kept in a dark condition for 2 h, the absorbance at a wavelength of 655 nm of the solution was recorded using UV-vis spectrophotometry. The concentration-absorbance standard curve was calibrated with different concentrations of ammonium chloride standard solution.

Determination of nitrite ions (NO_2^--N)

UV-vis spectrophotometer was used to quantify the NO_2^- concentration in the electrolyte before and after testing. First, to prepare the color reagent, 4 g of p-aminobenzenesulfonamide was added to a mixture of 50 mL deionized water and 10 mL phosphoric acid, followed by dissolution of 0.2 g N-(1-naphthyl) ethylenediamine dihydrochloride. The resulting solution was transferred to a 100 mL volumetric flask and diluted to volume with deionized water. Before UV-vis measurement, the electrolyte was collected and diluted to the detection concentration range, after that, 3 mL 1 M HCl and 0.1 mL of the color reagent was added to the diluted electrolyte. After thorough mixing and standing at room temperature for 20 minutes under ambient and dark conditions, the absorbance at a wavelength of 540 nm of the solution was recorded using UV-vis spectrophotometry. The concentration–absorbance curve was calibrated using a series of standard potassium nitrite solutions with linear fitting prepared beforehand. NO_2^- product concentrations were calculated based on the tested absorbance and the standard curve.

Determination of NO_3^--N

First, a certain amount of electrolyte was collected and diluted to the detection range. Then, Add 1.0 mL of 1 mol/L HCl and 0.1 ml of 0.8 wt % sulfamic acid solution to the diluted 4 ml electrolyte above. The absorption spectrum was measured using an UV−Vis spectrophotometer and the absorption intensity at a wavelength of 220 and 275 nm was recorded. The absorption at 220 and 275 nm was caused by nitrate and organic matter, respectively. The final absorbance value was calculated by this equation: $A = A_{220\ nm}-2A_{275\ nm}$. The concentration−absorbance curve was calibrated by a series of standard Sodium nitrate solution.

Isotope labelling experiment

Using $K^{15}NO_3$ (^{15}N-labeled potassium nitrate, Macklin Co., Ltd, with a purity of >99.0%) as the feed nitrogen source, the isotope labeled NITRR was carried out to determine the source of NH_3. 1 M KOH was used as the electrolyte, and 100 mM $K^{15}NO_3$ was added to the cathodic compartment as the reactant. 1H nuclear magnetic resonance (NMR) spectroscopy was employed to confirm the $^{15}NH_4^+$ and $^{14}NH_4^+$. In a standard procedure, 250 μL of the tested electrolyte was initially diluted to bring it

within the detection range and adjusted to a pH of 2.0 by adding 4 M HCl. Subsequently, the solution was mixed with 250 μL of DMSO-d6 (hexadeuterodimethyl sulfoxide, Shanghai Macklin Biochemical Technology Co., Ltd., with a purity of 99.9%), which included 10 mM $C_4H_4O_4$ (maleic acid, Shanghai Macklin Biochemical Technology Co., Ltd., with a purity of ≥ 99.0%). DMSO-d6 served as the solvent, and $C_4H_4O_4$ acted as the internal standard. Finally, the prepared solution was analyzed using a 600 MHz NMR spectrometer.

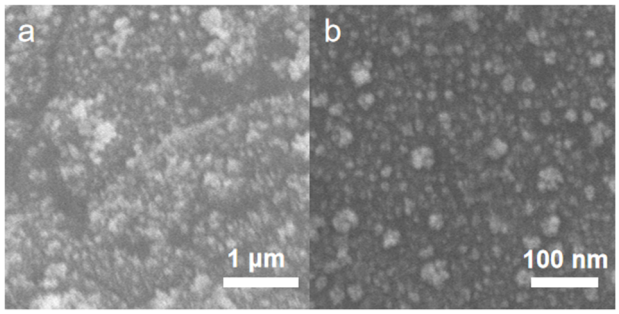

Figure S1. SEM image of Ag particles.

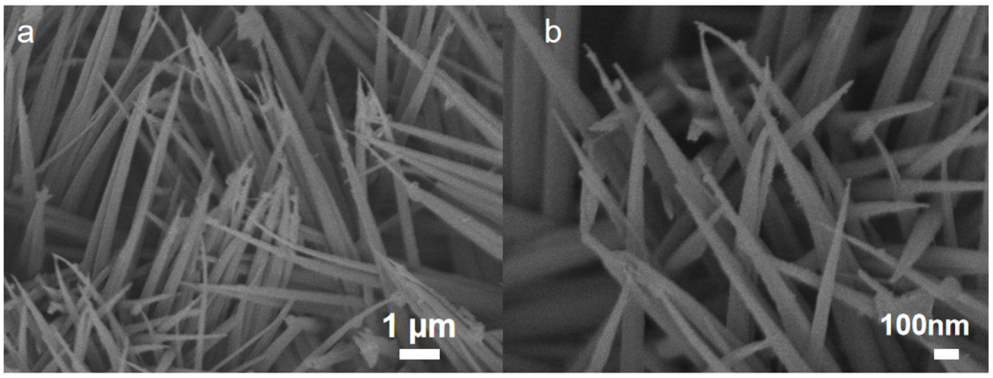

Figure S2. SEM image of $Co(OH)_2$ nanowires.

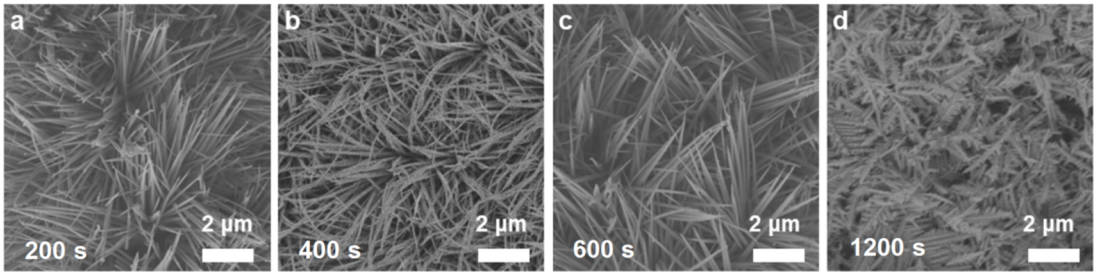

Figure S3. (a–d) and show SEM images of Ag/$Co(OH)_2$ NWs prepared after different electrodeposition times.

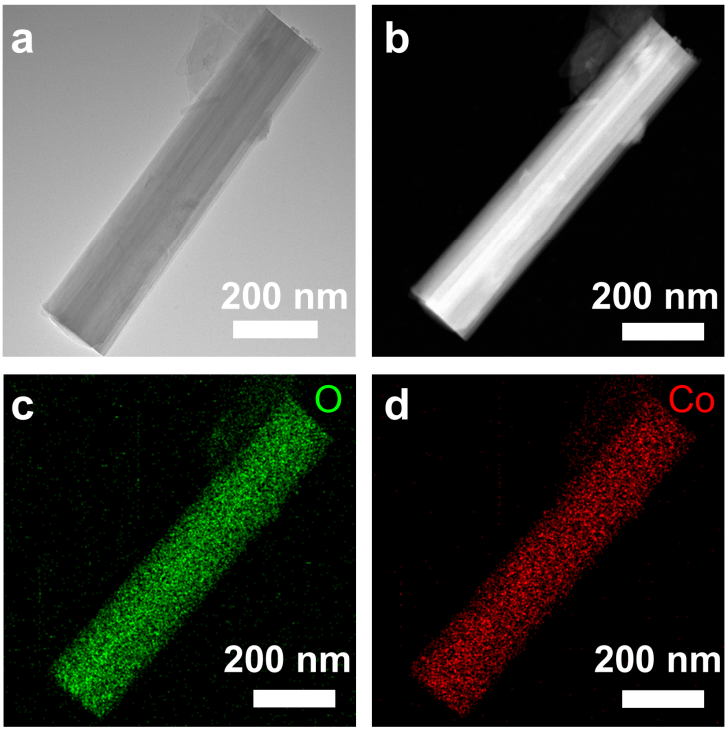

Figure S4. (a) TEM image of $Co(OH)_2$ NWs; (b–d) STEM images and corresponding elemental mapping maps.

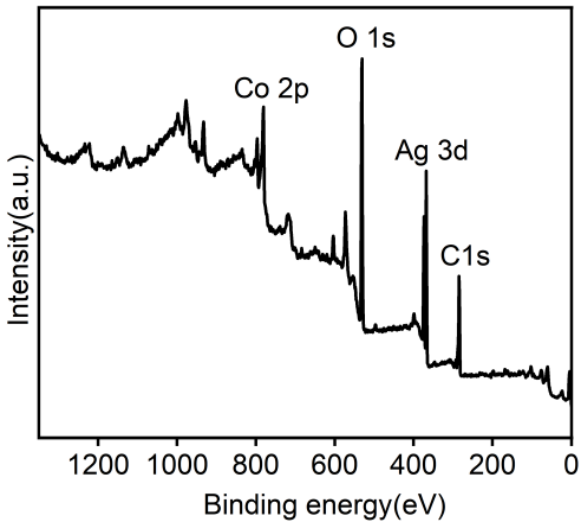

Figure S5. XPS survey spectrum of $Ag/Co(OH)_2$.

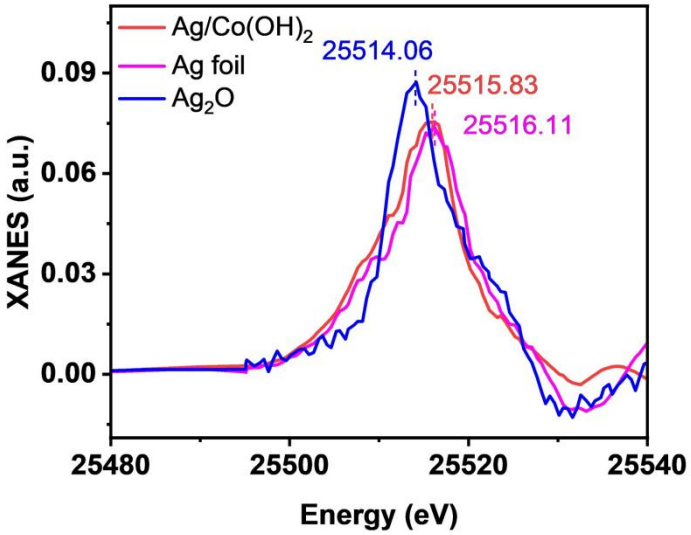

Figure S6. Corresponding first-derivative XANES curves at the Ag K-edge of $Ag/Co(OH)_2$, Ag foil, and Ag_2O.

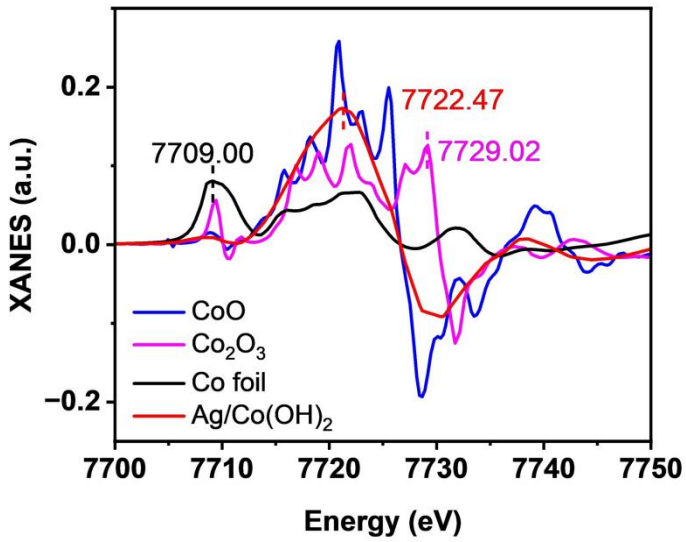

Figure S7. Corresponding first-derivative XANES curves at the Ag K-edge of $Ag/Co(OH)_2$, Co foil, CoO, and Co_2O_3.

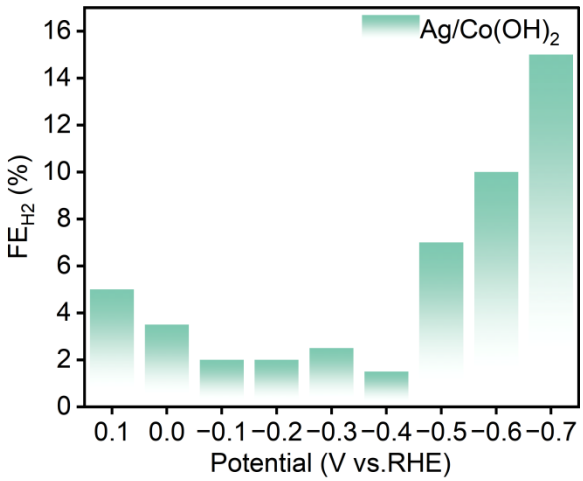

Figure S8. Faradaic efficiencies of H_2 over the $Ag/Co(OH)_2$ catalyst at different applied potentials (V vs. RHE).

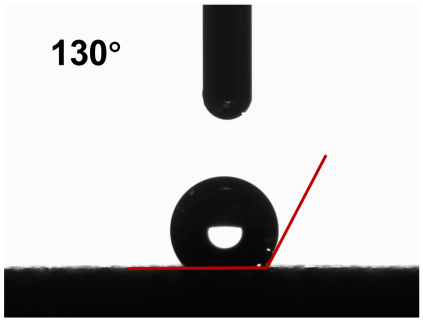

Figure S9. Photograph of the contact angle measurement for an electrolyte droplet on copper foam.

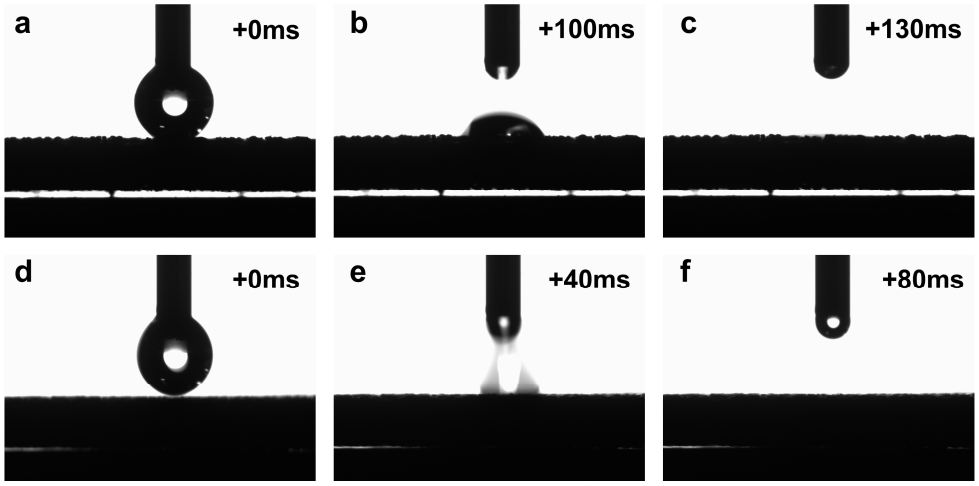

Figure S10. Photographs of the electrolyte droplet before (a) and after (b, c) $Co(OH)_2$ NWs; photographs of the electrolyte droplet before (d) and after (e, f) $Ag/Co(OH)_2$ NWs.

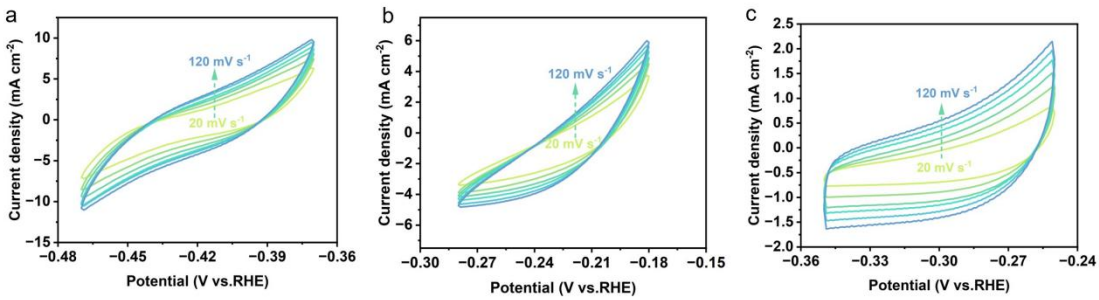

Figure S11. Cyclic voltammetry curves of (a) Ag/$Co(OH)_2$, (b) $Co(OH)_2$ and (c) Ag electrodes at different scan rates.

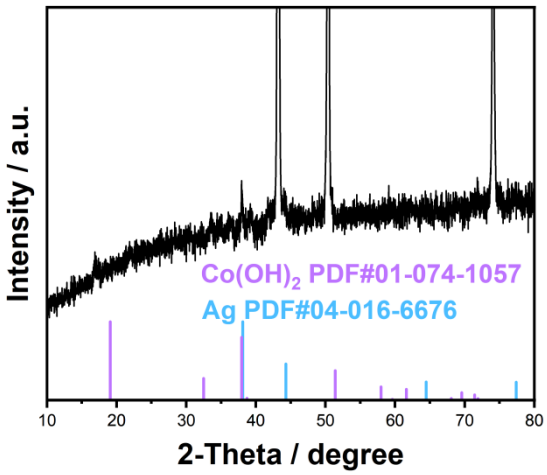

Figure S12. XRD of Ag/$Co(OH)_2$ NWs after reaction.

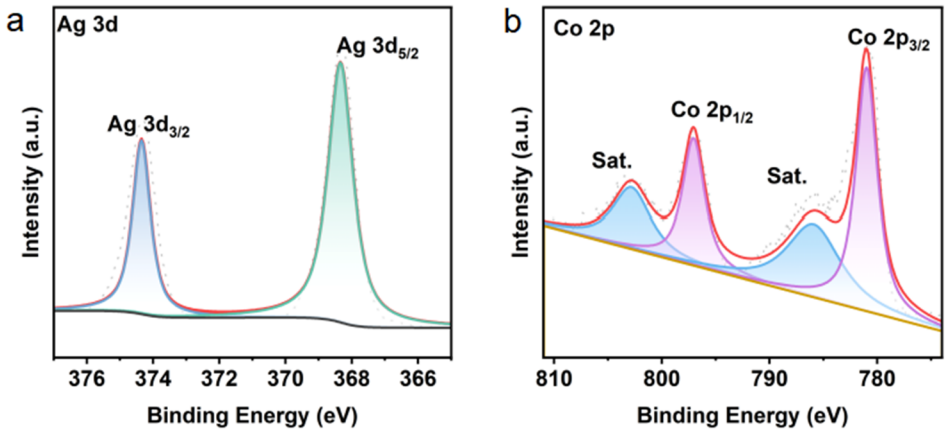

Figure S13. (a) Co 2p and (b) Ag 3d XPS spectra of Ag/$Co(OH)_2$ after reaction.

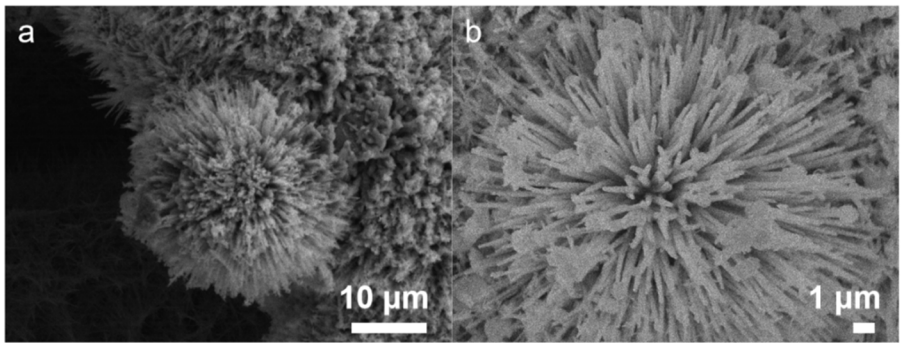

Figure S14. SEM image of $Ag/Co(OH)_2$ NWs after reaction.

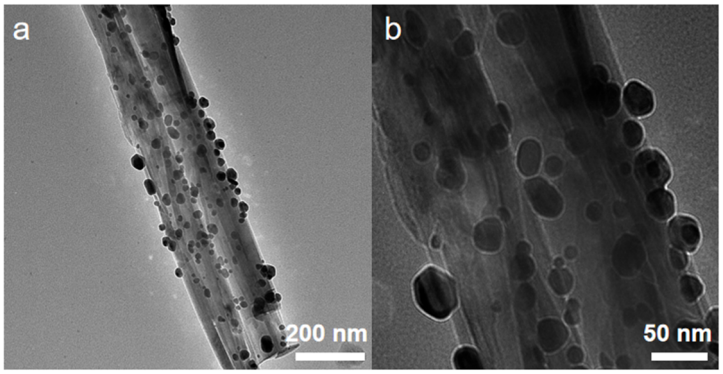

Figure S15. TEM image of $Ag/Co(OH)_2$ NWs after reaction.

Table S1. Comparison of Faradaic efficiency and yield between $Ag/Co(OH)_2$ NWs and recently reported catalysts.

Catalyst	Nitrate concentration	Potential (V vs. RHE)	FE (%)	Yield rate (mg_{NH3} h^{-1} cm^{-1})	Ref.
$Ag/Co(OH)_2$ NWs	0.1 M	-0.7	98.7	43.7	This work
$Ag_{1.5}Co/CC$	0.1 M	-0.75	96.11	4.25	[1]
$Ag@Cu_3N$	0.1 M	-0.3	95.9	32.4	[2]
Ag/Ag-Co	0.1 M	-0.3	97.1	25.1	[3]
Ni-MOFs@Ag	0.1 M	-0.2	90	2.07	[4]
Ag_{SA}-Cu NWs	0.1 M	-0.6	96.75	2.5	[5]
Ag/N-WO_3	0.16 M	-0.4	94	39.1	[6]
$Cu_2O+Co_3O_4$	1.0 M	-0.3	85.4	12.75	[7]
Cu-CoO/$Co(OH)_2$	0.1 M	-0.5	94.7	7.31	[8]
i-Ag/Co_3O_4 NWs	0.1 M	-0.25	94.3	4.3	[9]

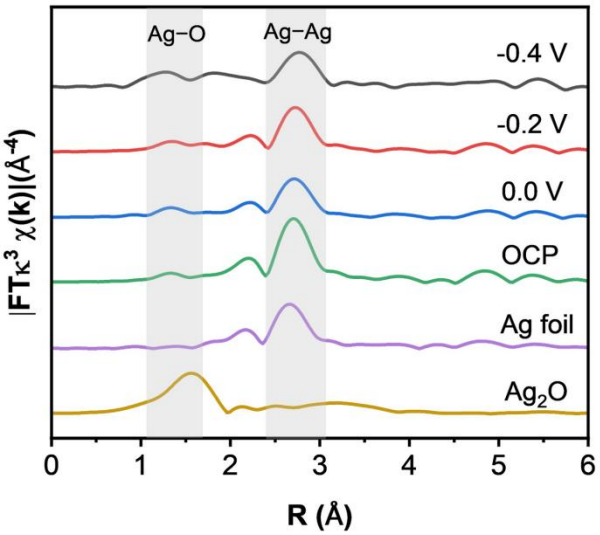

Figure S16. In-situ k^3-weighted FT-EXAFS spectra at Ag K-edge under various applied potentials, with Ag foil and Ag_2O as references.

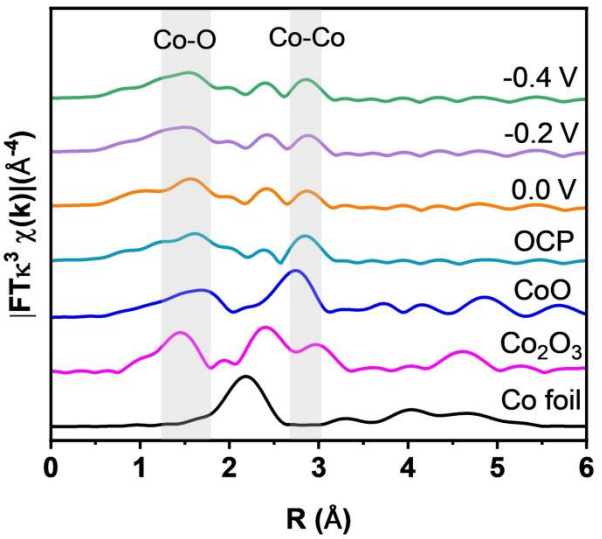

Figure S17. In-situ k^3-weighted FT-EXAFS spectra at Co K-edge under various applied potentials, with Co foil, CoO, and Co_2O_3 as references.

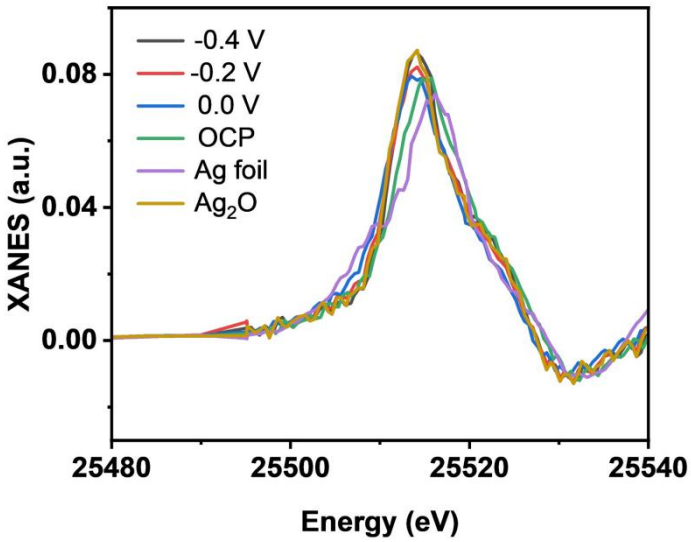

Figure S18. Corresponding first-derivative XANES curves at the in-situ Ag K-edge of $Ag/Co(OH)_2$ at different applied potentials.

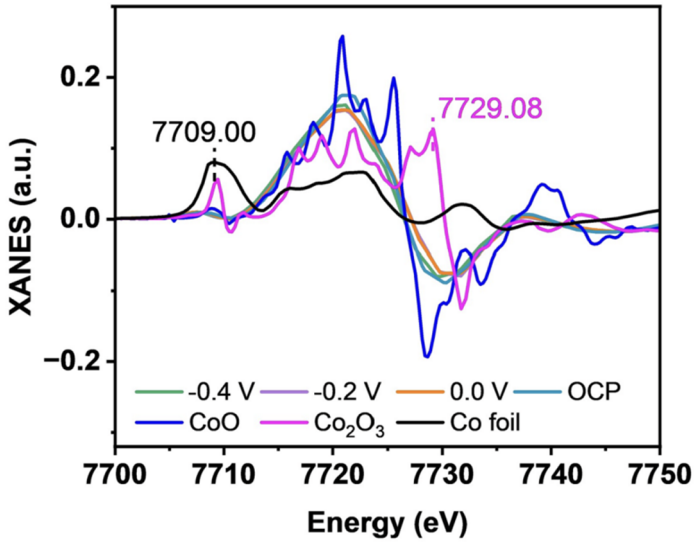

Figure S19. Corresponding first-derivative XANES curves at the in-situ Co K-edge of $Ag/Co(OH)_2$ at different applied potentials.

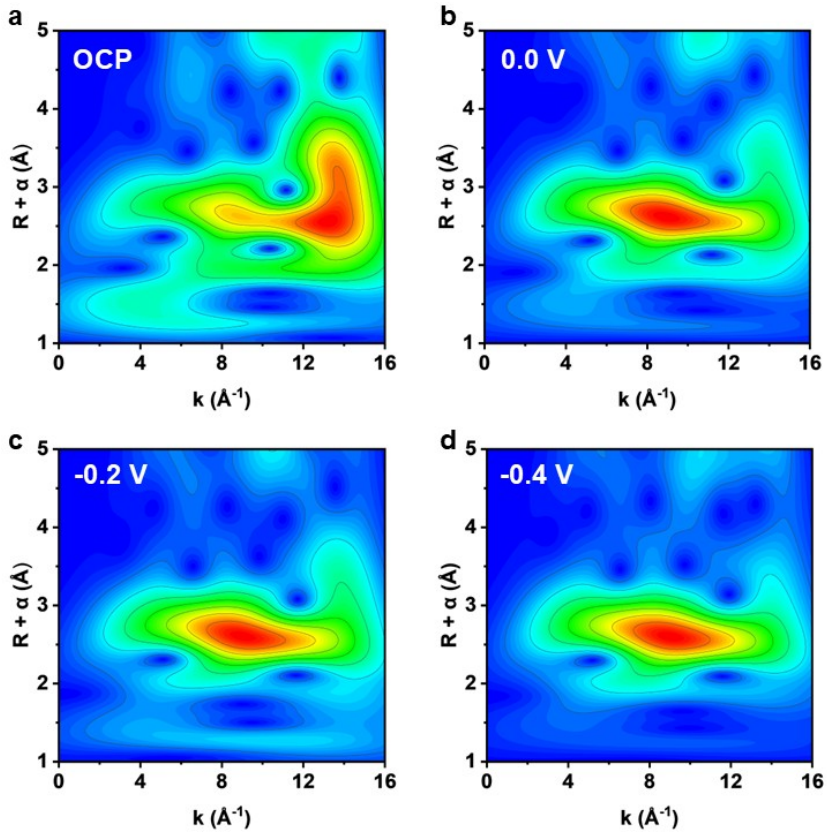

Figure S20. (a) Wavelet transform contour plot of in-situ Ag K-edge EXAFS for $Ag/Co(OH)_2$ at (a) OCP, (b) 0.0 V vs. RHE, (c) −0.2 V vs. RHE, and (d) −0.4 V vs. RHE.

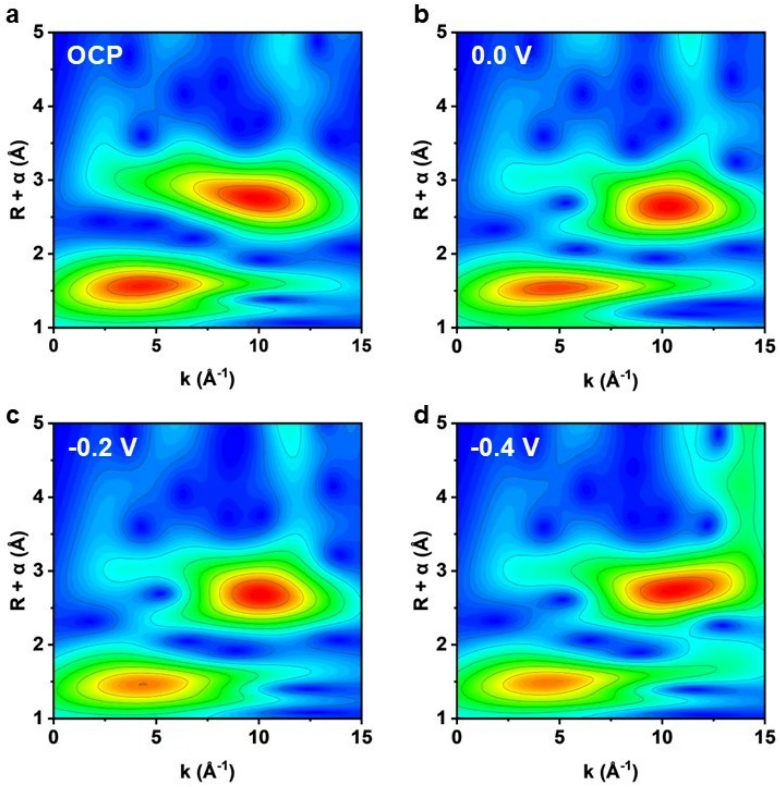

Figure S21. Wavelet transform contour plot of in-situ Co K-edge EXAFS for $Ag/Co(OH)_2$ at (a) OCP, (b) 0.0 V vs. RHE, (c) −0.2 V vs. RHE, and (d) −0.4 V vs. RHE.

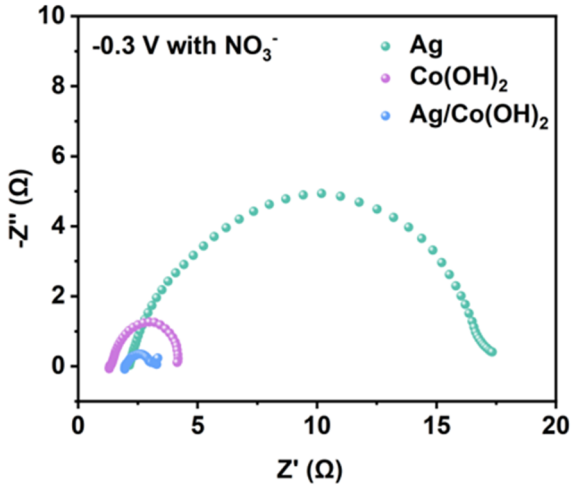

Figure S22. EIS curves for Ag/CF, $Co(OH)_2$ NWs, and $Ag/Co(OH)_2$ NWs.

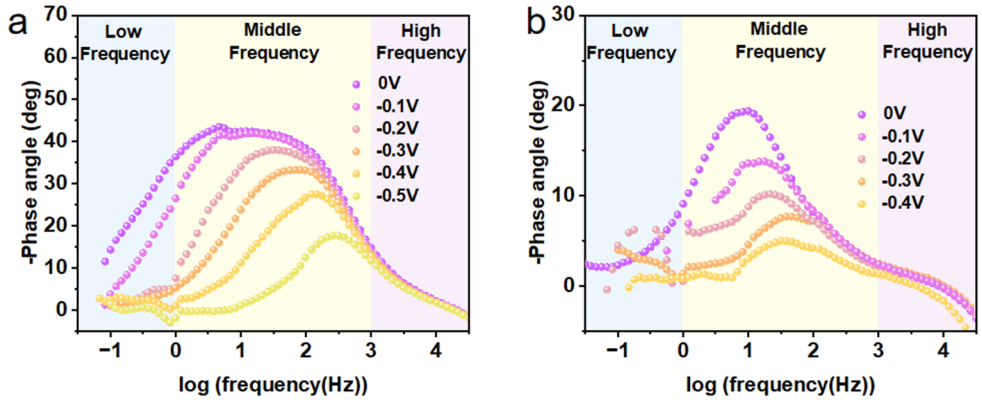

Figure S23. (a) Ag/CF; (b) In-situ Bode plot of $Co(OH)_2$ NWs in a potassium nitrate solution.

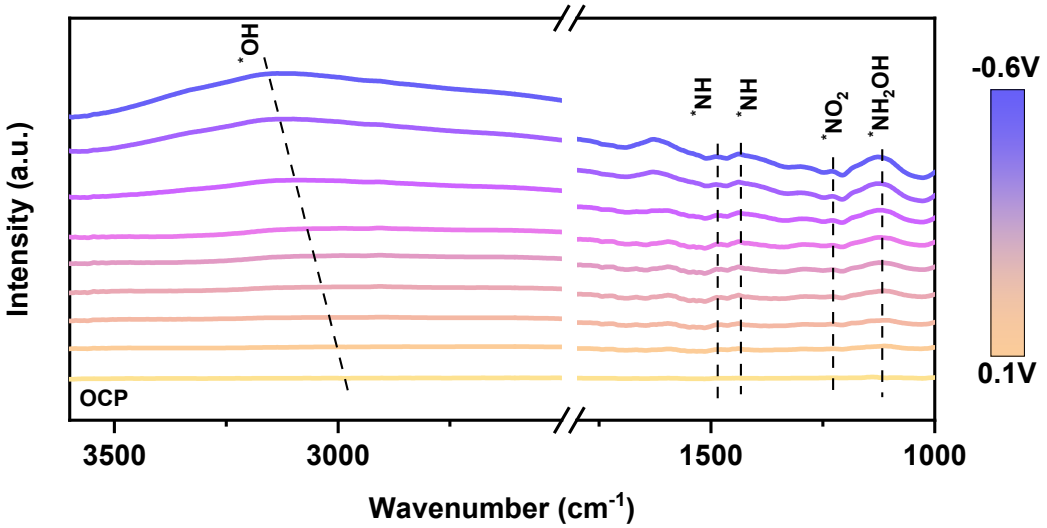

Figure S24. In-situ FTIR spectrum of $Co(OH)_2$ nanowires.

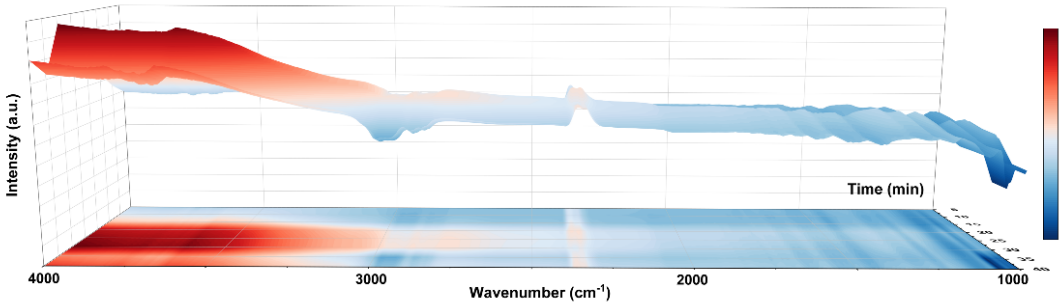

Figure S25. In situ FTIR spectra of $Ag/Co(OH)_2$ NWs.

Reference

1. Fan, Z.; Cao, C.; Yang, X.; et al. Interfacial electronic interactions promoted activation for nitrate electroreduction to ammonia over Ag-modified Co_3O_4. Angew. Chem. Int. Ed. **2024**, 63, e202410356.
2. Dong, H.; Ye, J.; Liu, X.; et al. Spatially separated Ag@Cu_3N tandem electrocatalyst with high nitrate-to-ammonia selectivity via decoupled deoxygenation-hydrogenation pathway. Adv. Funct. Mater. **2025**, e202526882.
3. Feng, Z.; He, Y.; Cui, Y.; et al. Efficient tandem electrocatalytic nitrate reduction to ammonia on bimodal nanoporous Ag/Ag-Co across broad nitrate concentrations. Nano Lett. **2024**, 24, 11929–11936.
4. Zhang, Y.; Ma, J.; Wang, B.; et al. Aldehyde directed in situ loading of Ag nanodots around the open metal sites of MOFs for the tandem catalysis of nitrate to ammonia. Small **2025**, 21, 2408602.
5. Liu, X.; Xiang, T.; Liu, J.; et al. Ag single atoms boosting water dissociation on Cu nanowires for efficient H*-mediated nitrate reduction at ultra-low concentrations with ammonia recovery. Adv. Funct. Mater. **2026**, 36, e21402.
6. Zhang, J.; He, W.; Quast, T.; et al. Single-entity electrochemistry unveils dynamic transformation during tandem catalysis of Cu_2O and Co_3O_4 for converting NO_3^- to NH_3. Angew. Chem. Int. Ed. **2023**, 62, e202214830.
7. Ren, Z.; Shi, K; Meng, Z.; et al. Complete single-pass conversion of dilute nitrate to ammonia using $Cu/Co(OH)_2$ tandem electrocatalyst. ACS Energy Lett. **2024**, 9, 3849–3858.
8. Wu, S.; Jiang, Y.; Luo, W.; et al. Ag-Co_3O_4-CoOOH-nanowires tandem catalyst for efficient electrocatalytic conversion of nitrate to ammonia at low overpotential via triple reactions. Adv. Sci. **2023**, 10, 2303789.